Ceramics International 43 (2017) 10057–10065

Contents lists available at ScienceDirect

Ceramics International

journal homepage: www.elsevier.com/locate/ceramint

The effect of silicon nitride powder characteristics on SiAlON microstructures, densification and phase assemblage

Selçuk Özcan[a], Gökhan Açıkbaş[b], Nurgül Özbay[a], Nurcan Çalış Açıkbaş[c,*]

[a] Department of Chemical and Process Engineering, Bilecik S.E. University, Bilecik, Turkey
[b] Metallurgy Program, Bilecik S.E. University, Bilecik, Turkey
[c] Department of Metallurgical and Materials Engineering, Bilecik S.E. University, Bilecik, Turkey

ARTICLE INFO

Keywords:
Si_3N_4 powder
SiAlON ceramics
Powder characterization
Milling
Microstructure

ABSTRACT

The surface characteristics, particle size distribution and impurities of starting Si_3N_4 powders exert a very significant influence on the microstructure of sintered silicon nitride based ceramics. Even a change of the processing conditions such as milling liquid media (water or isopropyl alcohol) and milling time can have a substantial effect on particle surface groups, and hence on the microstructure of sintered samples. In this study, SEM, XRD, FTIR, BET, elemental analysis and laser diffraction techniques were used for the comprehensive characterization of Si_3N_4 powders which were produced by diimide, direct nitridation and combustion synthesis, in as received state, and after milling in different liquid media (aqueous or alcohol), for various milling durations. The correlation of the surface characteristics and properties of the Si_3N_4 powders with sintering behavior, and microstructural evolution, densification and phase assemblages of the resulting SiAlON ceramics were reported. The milling conditions affected the surface chemistry of Si_3N_4 powders and the subsequent microstructural evolution. The microstructures evolved from the coarser β-Si_3N_4 powders were coarser, but the fine β-Si_3N_4 powders yielded a bimodal microstructure. The critical particle diameter of the β-Si_3N_4 powder for the formation of needle like SiAlON grains was determined to be less than 0.5 μm.

1. Introduction

Engineering ceramics have been employed for mechanical, chemical, thermal and high temperature applications, as alternatives to metals, with considerably longer life times [1,2]. One of the most widely studied and well known engineering ceramics is silicon nitride (Si_3N_4) suitable for high temperature structural applications, since it provides a good combination of mechanical, chemical and thermal properties [3,4]. SiAlON ceramics also constitute an alternative class of materials that have many attractive characteristic properties such as high strength, hardness, wear resistance, low thermal expansion, high thermal conductivity and consequently excellent thermal shock resistance [5–12].

The macroscopic features and behavior of SiAlON ceramics are strongly influenced by and very sensitive to the microstructural properties. The characteristics of starting Si_3N_4 powder for their synthesis determine the sintering behavior, and hence microstructural evolution and eventual material properties to a great extent [13–20]. Especially the silicon nitride powder particle size, particle size distribution, particle shape, particle surface area, particle surface groups and oxide content were shown to be effective which in turn were affected by milling conditions such as mill type and material, revolution rate, milling time, and milling liquid medium (water or isopropyl alcohol) [13,21–23]. The type and amount of sintering additives and sintering conditions also have crucial importance on microstructural evolution, densification and phase assemblage of SiAlON ceramics, as well [24–27].

In this study, SEM, XRD, FTIR, BET, elemental analysis and laser diffraction techniques were used for comprehensive characterization of Si_3N_4 powders in the as received and milled states. The correlation of the surface characteristics of the Si_3N_4 powder with the sintering behavior, and microstructures, densification and phase assemblage of the resulting SiAlON ceramics was reported.

2. Materials and methods

Silicon nitride powders were obtained from three different manufacturers which were produced by diimide, direct nitridation, or combustion synthesis followed by milling in various liquid media (aqueous or alcohol). The powders were coded as R, A, and B. The

* Corresponding author.
E-mail address: nurcan.acikbas@bilecik.edu.tr (N.Ç. Açıkbaş).

http://dx.doi.org/10.1016/j.ceramint.2017.05.024
Received 20 April 2017; Received in revised form 3 May 2017; Accepted 3 May 2017
Available online 04 May 2017

Table 1
Main specifications of starting Si_3N_4 powders.

Code	α:β ratio	Mean particle size (μm)	Manufacturer	Sythesis method
R	98α:2β	0.55	UBE Industries Ltd., Tokyo, Japan	Diimide
A	89α:11β	~2	SKW-Trostberg AG, Germany	Direct nitridation
B	100β	10	Beijing Chanlian-Dacheng Trade Co., Ltd., China	Combustion synthesis

main specifications of the powders are indicated in Table 1. Attrition milling in water or isopropanol was performed to decrease the average particle size of A and B starting powders. The powder coded as A was attrition milled in water at 1300 rpm for 7 h and the mean particle size decreased to ~1 μm (coded as A1). The powder coded as B was attrition milled in water at 1300 rpm for 4 h and 21 h reducing the mean particle sizes to 2 μm and 0.5 μm, respectively (B2 and B05). In order to determine the milling liquid medium effect on the powder surface characteristics, the powder B was also milled in isopropanol at 1300 rpm for 9 h reducing the mean particle size to 1 μm (B1). The corresponding milled powders were coded as B2 (d50: 2 μm), B1 (d50: 1 μm) and B05 (d50: 0.5 μm).

The α:β-Si_3N_4 phase ratios were determined by using the area integrated intensities of the (102) and (210) reflections of α-Si_3N_4 and the (101) and (210) reflections of β-Si_3N_4 in the x-ray diffraction patterns (XRD-Panalytical, Empyrean with Cu-Kα radiation) as given in Eq. (1).

$$\frac{I_\beta}{I_\beta + I_\alpha} = \frac{1}{1 + K[(1/w_\beta) - 1]} \quad (1)$$

where I_α *and* I_β are the observed intensities of α and β-Si_3N_4 peaks, respectively, w_β is the relative weight fraction of β-Si_3N_4, and K is the combined proportionality constant given by Eq. (2) and Eq. (3).

$$I_\beta = K_\beta W_\beta \quad (2)$$

$$I_\alpha = K_\alpha W_\alpha \quad (3)$$

which are 0.518 for β (101) – α (102) reflections, and 0.544 for β (210) – α (210) reflections [28].

The particle sizes and shapes of the Si_3N_4 powders were determined by the scanning electron microscope (SEM-ZEISS Supra 40VP) secondary electron imaging. Prior to the SEM imaging the powders were dispersed in alcohol with ultrasonication, and sputter coated with Au-Pd to avoid electrical charging.

The particle size distribution of the as received and milled powders were determined by laser diffraction particle size analyzer (Malvern Mastersizer 2000) in a liquid medium, with the addition of small amounts of dispersant to avoid agglomeration. The measurement range of the instrument was given as 0.02–2000 μm. BET analysis was carried out to measure the specific surface area of the Si_3N_4 powders (Micromeritics, Asap 2020).

The possible chemical bonds were determined by Fourier transform infrared spectroscopy (FTIR) in the ATR mode (Perkin Elmer, Spectrum 100). Each spectrum was formed as the spectral average of at least four scans in the 400–4000 cm^{-1} range. Total oxygen content of the powders was determined by the inert gas fusion method using an elemental analyzer (LECO, EF400, USA).

30α^1:70β^1 SiAlON composition were produced with 9Y:0.5Sm:0.5Ca cation system and 2 mol% IGP content. All of the designed SiAlON compositions synthesized with different Si_3N_4 powders that were attrition milled using Si_3N_4 balls in water or isopropanol media. $CaCO_3$ (> 99.75%, Reidel-de Haen, Germany), Y_2O_3 (> 99.9%, H.C. Starck Berlin, Germany), Sm_2O_3 (> 99.9%, Stanford Materials Corp., USA) were used as sintering additives. CaO was used to avoid α^1 to β^1-SiAlON transformation, Y_2O_3 and/or Re_2O_3 (where $Z_{Re} \geq 62$) were used to increase the stability and hardness of α^1-SiAlON, and Sm_2O_3 (where $Z_{Re} < 62$) was used to develop elongated β^1-SiAlON grains and to increase fracture toughness. Si_3N_4 powders and sintering additives were mixed with high purity AlN powder with 1.6 wt% O content (H Type, Tokuyama Corp. Japan) and Al_2O_3 (Alcoa A16-SG Pittsburgh, USA). The green samples were prepared by uniaxially pressing the SiAlON powders at 25 MPa, followed by cold isostatic pressing at 300 MPa to obtain a homogeneous density. The samples were then sintered by gas-pressure sintering under 2.2 MPa nitrogen gas pressure. The weight loss and shrinkage of the sintered samples were determined, and Archimedes principle was utilized to measure their density. The phase ratios of α^1:β^1-SiAlON ceramics were determined by x-ray diffraction analysis by Eqs. (1)–(3). The microstructural analysis of the sintered samples was carried out by SEM back-scattered electron imaging (Zeiss VP40-Supra). The surfaces of the samples were polished to 1 μm, and sputter coated with Au-Pd prior to examination.

3. Results and discussion

3.1. Characterization of the initial Si_3N_4 powders

The properties of the powder pressed and sintered ceramic products are, in general, known to be affected by the chemical composition, phases, particle size distribution, particle shape, and impurity content of the raw materials. For instance, finer powders can be used to obtain denser materials. In the study, three different commercial silicon nitride powders which were synthesized by different production methods, were characterized and used.

The particle size distributions of the as received Si_3N_4 powders are given in Fig. 1. The mean particle sizes of the powders B, A, and R were

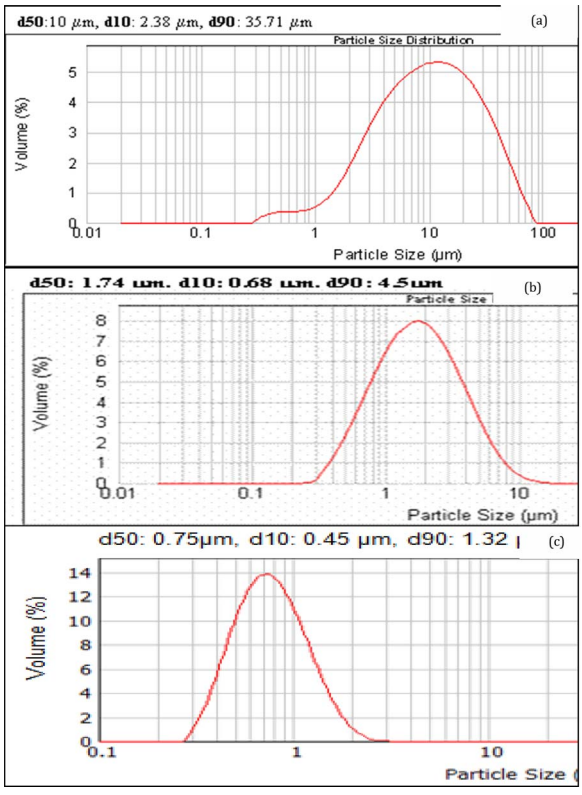

Fig. 1. Particle size distribution of starting Si_3N_4 powders (a) Beijing β-Si_3N_4 powder (coded B), (b) Silzot α-Si_3N_4 powder (coded A) and (c) UBE SN E-10 α-Si_3N_4 powder (coded R).

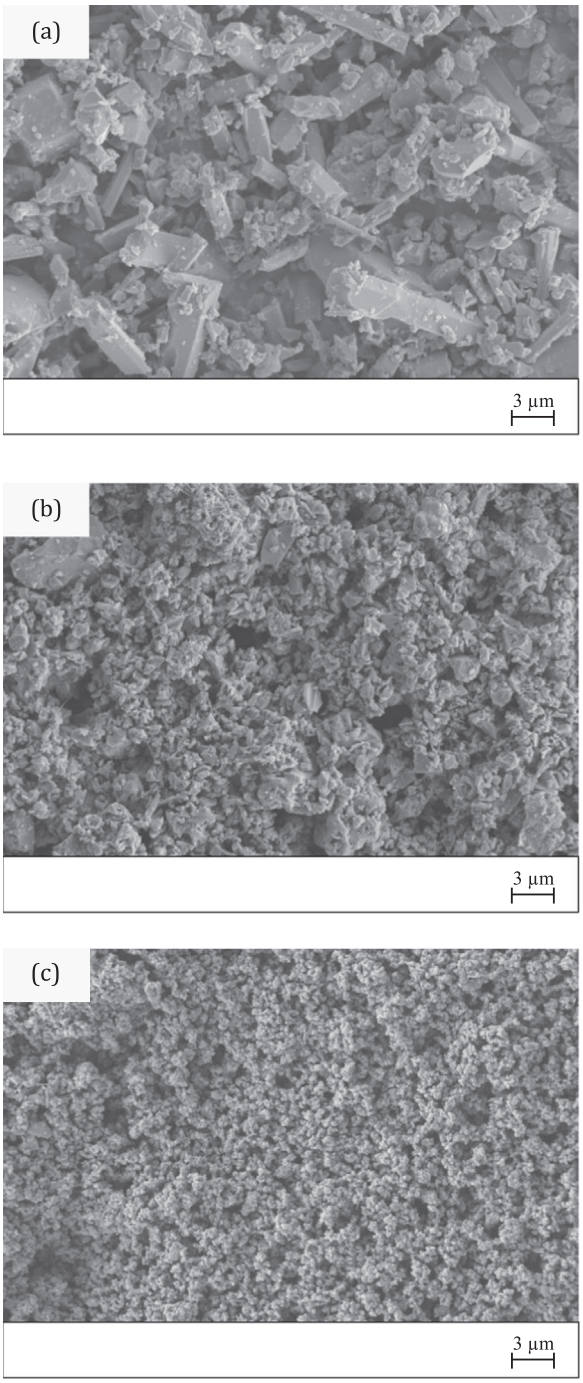

Fig. 2. SE-SEM images of starting Si_3N_4 powders (a) Beijing β- Si_3N_4powder (coded B), (b) Silzot α-Si_3N_4 powder (coded A) and (c) UBE SN E-10 α- Si_3N_4 powder (coded R).

measured as 10 μm, 1.74 μm, and 0.45 μm, respectively, by laser diffraction. Since the degree of initial agglomeration and breaking of the agglomerates by ultrasonication during the dispersion might affect the particle size distribution, SEM analysis was conducted to determine the particle sizes and shapes decisively. The SE-SEM images are given in Fig. 2. SEM analysis showed that the powder B had prismatic particle shape with an aspect ratio (legth/diameter) of ≥4.5 as seen in Fig. 2a. The powder A particle sizes were in between 1 to 2 μm, and particle shapes were various (sharp edges and prismatic) as in Fig. 2b. The R coded α-Si_3N_4 powder primary particle size was very fine, ~0.6 μm, with equiaxed particles. The prismatic or equiaxed shapes of the Si_3N_4 powders affect the dissolution of the particles during sintering. In general, while β-Si_3N_4 particles were prismatic in shape and stable, α-Si_3N_4 particles were equiaxed and easily dissolved.

3.2. The effect of milling parameters on silicon nitride powder characteristics

The commercial powders were ground in the attrition mill to obtain finer particle size distributions, and the ground powders were used to determine the effect of the particle size. Nevertheless, surface characteristics of powders could have changed with the milling parameters such as milling liquid medium and time. The surface characteristics of the powders are known to change sintering behavior, and therefore microstructure, phase assemblage, density, weight loss and shrinkage of sintered products. In order to determine the effect of particle surface characteristics on the densification and phase assemblage, the coarser A and B coded samples were milled in aqueous or isopropanol media for different milling durations. Particle size distribution and surface areas of powders are given in Table 2.

The powders were examined with the SEM-SE detector to determine the particle sizes and shapes, and the related images are given in Fig. 3. The particle size distributions of the milled powders were obtained by the laser diffraction technique, and the graphs are given in Fig. 4. The powder A1, which was obtained by the milling of the powder A in the attrition mill for 7 h at 1300 rpm in water medium, had a rather uniform particle size of approximately 1 μm of varying shapes as seen in Fig. 3a. The particle size distribution was in a relatively narrow range of 0.58–2.7 μm with a mean size of 1.22 μm as given in Fig. 4a. With milling the surface area increased from 4.85 m^2/g of the powder A to 6.45 m^2/g of the powder A1 as determined by BET.

In order to determine the effect of the milling medium on the final properties, the coarse powder B was milled alternatively in isopropanol and also in water. The powder coded as B2 was obtained as the result of milling in water for 4 hrs at 1300 rpm, and the particles had prismatic shapes in the most part, and had a wide particle size range of approximately 0.5–5 μm as can be seen in the SEM image (Fig. 3b). The laser diffraction revealed a wide particle size distribution in the 0.7–4.8 μm range indicating a mean of 2.1 μm (Fig. 4b). The powder coded as B1 was obtained by milling in isopropanol for 9 hrs at 1300 rpm. The powder B1 particles had prismatic and near equiaxed shapes of approximately 0.5–2 μm in size as seen in Fig. 3c. The laser diffraction particle size distribution graph indicated a mean particle size of 1.15 μm in the range of 0.54–2.4 μm (Fig. 4c). The surface area

Table 2
Milling parameters, particle size distributions and surface area of Si_3N_4 powders.

Milling conditions	***R*** None	***A*** None	***A1*** Attrition milling in water, 7 h, 1300 rpm	***B*** None	***B2*** Attrition milling in water, 4 h, 1300 rpm	***B1*** Attrition milling in isopropanol, 9 h, 1300 rpm	***B0.5*** Attrition milling in water, 21 h, 1400 rpm
D50	0.75	1.70	1.22	10	2.10	1.15	0.53
D10	0.45	0.70	0.58	2.40	0.54	0.20	0.20
D90	1.32	4.50	2.70	36	2.43	1.40	1.40
BET (m^2/g)	9.69	4.85	6.45	–	–	19.21	28.60

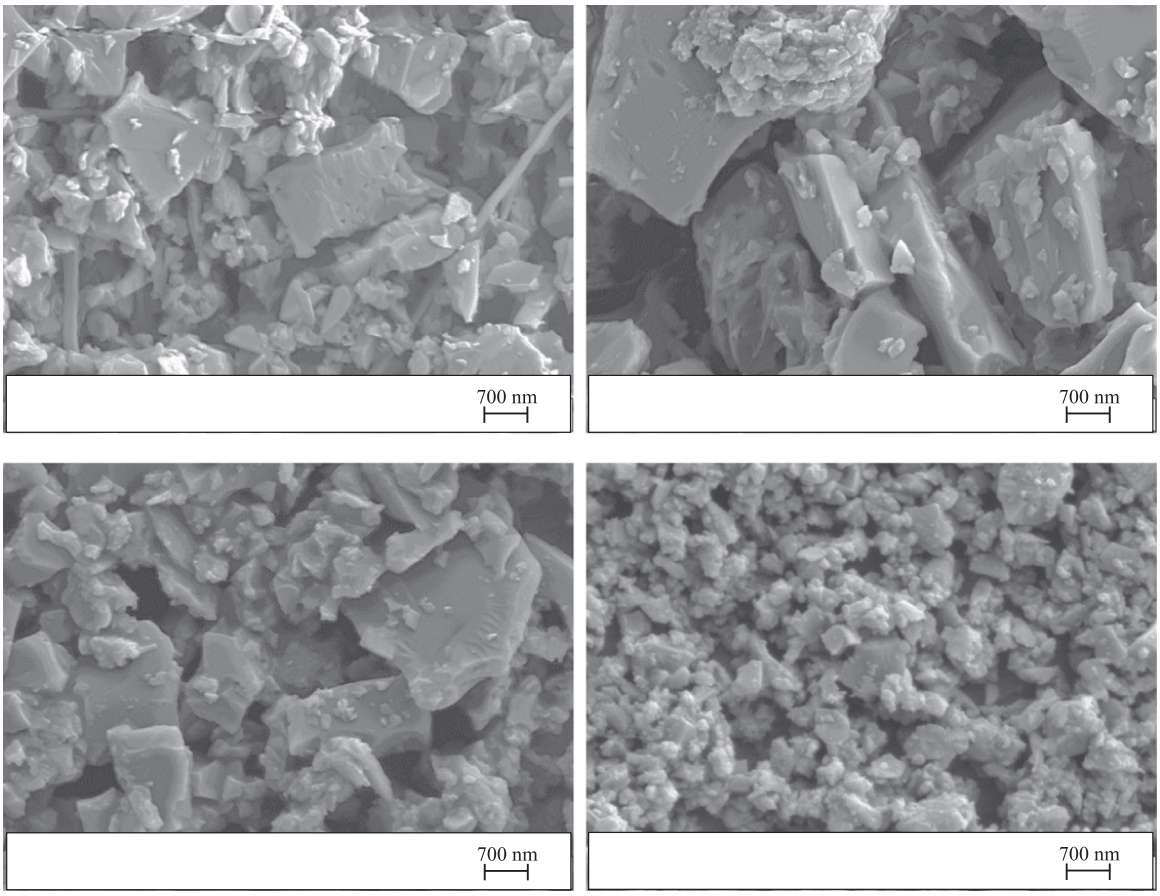

Fig. 3. SEM-SE image of milled Si_3N_4 powders which were coded as (a) A1, (b) B2, (c) B1 and (d) B05.

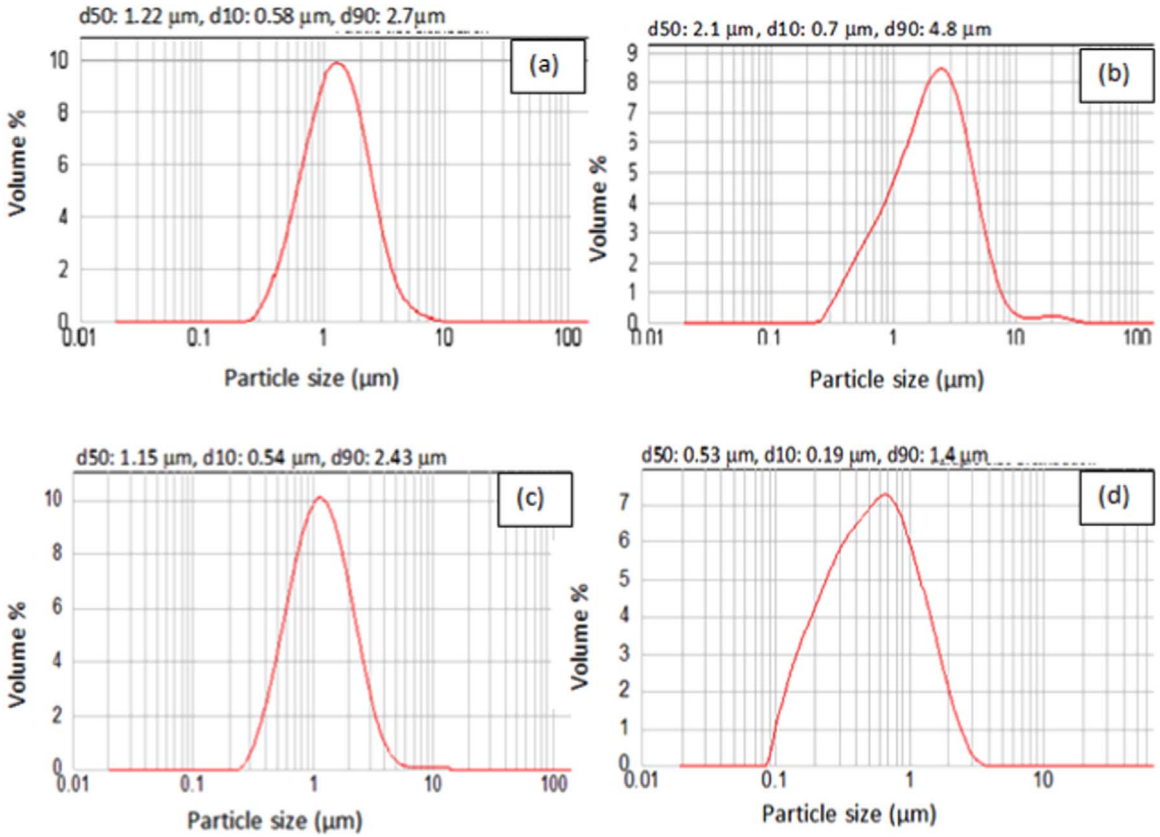

Fig. 4. Particle size distribution graph of milled Si_3N_4 powders, (a) A1, (b) B2, (c) B1 and (d) B05.

was 19.21 m^2/g. The powder B0.5, which was produced by milling in water for 21 h at 1400 rpm, consisted of fine, equiaxed, sharp edged particles (Fig. 3d) with a particle size distribution of 0.19–1.4 μm and a mean of 0.53 μm as determined by the laser diffraction (Fig. 4.d). The surface area was found as 28.6 m^2/g.

In order to investigate the effect of milling on the phase evolution of the powders, the XRD analyses of the commercial and milled powders were carried out. The XRD patterns are given in Figs. 5a and 5b. α:β-Si_3N_4 phase ratios were not changed by the milling as might be expected. The commercial powder A contained Si as impurity, but the related peak intensity decreased significantly after milling. Also the impurities Si and $FeSi_2$ contained in the commercial powder B were reduced by the milling operation as evidenced by their curtailed XRD peak intensities. However, in the extensively milled B0.5 powder SiO_2 was detected which might have been due to the reaction given in Eq. (4).

$$Si_3N_4 + 6H_2O \rightarrow 3SiO_{2(amorphous)} + 4NH_3 \quad (4)$$

The oxygen content of the Si_3N_4 powder was determined by elemental analysis (Leco analyzer). After the milling, the oxygen contents of the powders A1, B2, B1 and B0.5 powders were determined as 1 wt%, 3 wt%, 4 wt% and 8 wt%, respectively. Therefore the existence of a correlation between the increasing milling duration and the increasing oxygen content of the β-Si_3N_4 powders was revealed.

The surface characteristics of the Si_3N_4 powders were determined by the FTIR analyses. The spectra taken in the ATR mode in the 400–4000 cm^{-1} are given in Fig. 6 and the results are summarized in Table 3. Each spectrum was a spectral average of at least four scans. The bands due to the atmospheric contributions of water vapor and CO_2 were subtracted from the spectra in order to improve the spectral quality. The alpha phase powders (*R* and A) exhibited vibrational fingerprints between 450 cm^{-1} and 920 cm^{-1} with four sharp peaks at 459 cm^{-1}, 462 cm^{-1}, 599 cm^{-1}, and 683 cm^{-1} (Figs. 6a and b) which were consistent with the Si-N stretch in SiN_3 as provided in the literature [29] and in conformity with the XRD result indicating the existence of α-Si_3N_4 phase. The band at 3435 cm^{-1} was ascribable to υ(O-H) stretch of hydroxyl groups and yielded strong peaks only for B0.5 powder providing evidence of absorbed water (Fig. 6c). The band

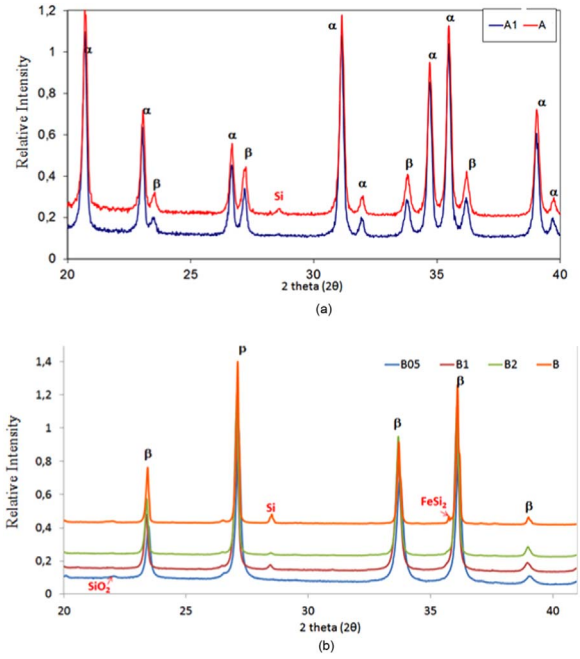

Fig. 5. XRD spectra of as received and milled Si_3N_4 powders (a) A and A1, (b) B, B2, B1 and B05.

at around 1036 cm^{-1} in the spectra of B0.5, B1, and B2 powders was attributed to the asymmetric stretch mode of the Si–O–Si bond (Fig. 6d). The bands in the region 600–900 cm^{-1} were associated with Si-N stretch in Si_3N_4. The broad band centered around 814–900 cm^{-1} corresponded to the Si-N stretch in β-Si_3N_4 as given in Fig. 6d.

3.3. Effect of Si_3N_4 powder surface characteristics on the microstructure, densification, and phase assemblage of SiAlON ceramics

Generally, in colloidal processing the surface characteristics of the powders have crucial effects on the microstructure, densification, and phase assemblage. As a result of the sintering of the compositions prepared by the powders R and A1, 99.7% theoretical density was reached, while with the compositions comprising the powder A the density after sintering remained as 97.6% of the theoretical lower than the targeted. The initially designed α^1:β^1 SiAlON phase ratios were obtained with the powders R and A1 as approximately 30α^1:70β^1, and melilite phase crystallization was achieved. The weight loss was around 1.3% with both of the compositions (Table 4).

The commercial β-Si_3N_4 powder was ground resulting in various particle size distributions with the approximate means of 2 μm (B2), 1 μm (B1) and 0.5 μm (B0.5) and compositions were prepared with these milled powders. These compositions were sintered at 1940 °C for 2 h under 2.2 MPa N_2 gas pressure. The density measurements indicated that over 99.5% of the theoretical densities were achieved. Although the mean particle size of the powder B2 was ~2 μm a dense sintered material was produced due to the impurities contained in the initial powder which in turn resulted in the formation of a higher quantity of high temperature liquid phase. In the literature it was reported that the impurities contained in the powders caused low eutectic temperatures, assisting sintering [30].

The sintering shrinkages were found to be 14.3% for B2, 17.0% for B1, and 18.4% for B0.5 samples. The shrinkages increased with decreasing particle size as expected [19]. For the compositions prepared by the powders B2 and B1, the initially designed 30α^1:70β^1 SiAlON phase ratios were approached, and the melilite crystallization was observed. However, for the composition prepared with the powder B0.5, α^1-SiAlON phase stability and the melilite phase crystallization were not achieved. Since the powder B0.5 was obtained by the milling of the commercial β-Si_3N_4 powder in the attrition mill for 21 h at 1400 rpm in water medium, Si_3N_4 reacted with water yielding SiO_2 and NH_3 as the reaction products given by Eq. (4).

As determined by the elemental analysis the oxygen content of the as received β-Si_3N_4 powder was 3 wt%, and raised to ~8 wt% for the powder B0.5. The formation of SiO_2 on the surface of the β-Si_3N_4 grains caused the composition to shift from 70β to 100β-SiAlON as could be seen in the phase diagram given elsewhere [14]. Oxide layer formation on Si_3N_4 powder surface was reported to depend on temperature [31]. The dissolution progressed at a high rate at temperatures above 40 °C. SiO_2 formed on the surface, redissolved, and started to reform on the new surfaces. Nevertheless, the crystallization of the nitrogen rich melilite phase was inhibited since the grain boundary phase was rich in oxygen. For this composition in order to stabilize the α^1-SiAlON phase the composition was modified, however, the oxygen content was too high (~8 wt%) to achieve the required ratio.

The finer particle size powders B0.5 and R were sintered at 1850 °C, for 1 h, under 2.2 MPa N_2 gas pressure, and yielded finer microstructures as confirmed by the literature [32]. Therefore, the fine microstructure achieved might prove convenient for wear resistant applications [33–43]. While after sintering the density of R composition reached 98.8% of the theoretical, the composition containing the powder B0.5 densified to 99.43% of the theoretical since it was hydrolyzed during milling and became rich in oxygen. During the sintering of the R composition since the melilite phase formation was extensive and did not completely fuse at the sintering temperature, the

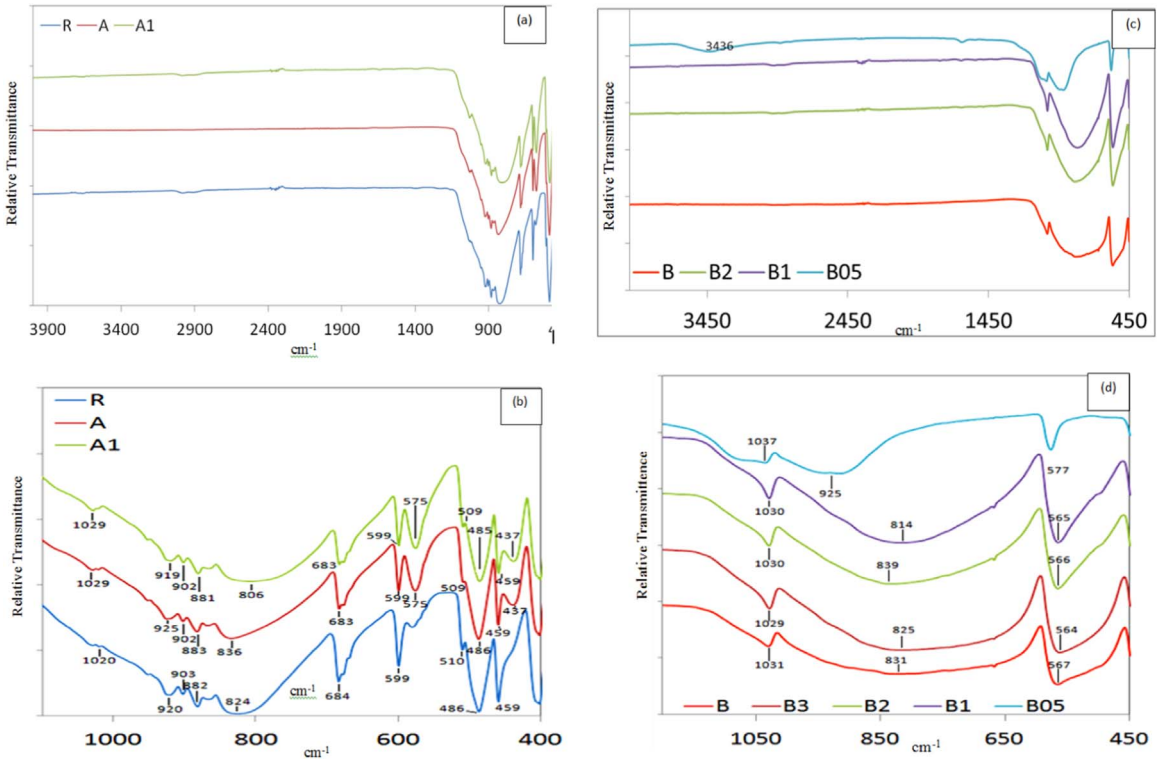

Fig. 6. FTIR spectrums of Si_3N_4 powders (a, b) UBE SN E-10 α-Si_3N_4 powder (coded as R) and as-received and milled Silzot α-Si_3N_4 powders (coded as A, A1), (c, d) as-received and milled state of Beijing β-Si_3N_4 powders (coded as B, B2, B1, B05).

Table 3
Band assignments for FTIR spectra of Si_3N_4 powders.

Wave number (cm^{-1})	Groups	R	A	A1	B	B2	B1	B05
3435	OH	–	–	–	–	–	–	+
1036–1028	Si-O-Si	+	+	+	+	+	+	+
925–900	Si-N	+	+	+	–	–	–	–
835–814	Si-N	+	+	+	+	+	+	–
683–599	Si-N	+	+	+	–	–	–	–
580–563	Si-N	+	+	+	+	+	+	+
459	Si-N	+	+	+	–	–	–	–

densification was adversely affected. The powder B0.5, on the other hand, included SiO_2 as impurity and the fused phase had a very low eutectic point rendering sintering relatively easier. The sintering weight loss was a relatively high 3.7 wt% as the result of faster densification and the incorporated impurities. By the sintering of the R composition the initially designed α^1:β^1-SiAlON phase ratios was achieved, while by the sintering of the B0.5 powder the α-SiAlON was not stabilized because of its oxygen rich composition.

The SEM images of the microstructures obtained by the sintering of the R and the A1 powder containing compositions at 1940 °C for 2 h under 2.2 MPa N_2 gas pressure, are given in Fig. 7. Since the R powder had a finer particle size in comparison to the A1 powder, its solubility in the fused phase was higher and the needle like β^1-SiAlON grains

Table 4
Effects of powder surface characteristics on densification and phase assemblage.

Powder	Milling liquid	Milling time (h)	O (wt%)	FTIR groups	Si_3N_4 powder α:β ratio	Impurities	Sintering conditions	Final phases	%T.D.	%W.L.	% shrinkage
R	–	–	1.4	Si-N Si-O-Si	98α:2β		1940 °C, 2 h, 2.2 MPa N_2	66β^1:34α^1 Melilite	99.93	1.39	–
R	–	–	1.4	Si-N Si-O-Si	98α:2β		1850 °C, 1 h, 2.2 MPa N_2	71β^1:29α^1 Melilite	98.80	0.93	–
A	–	–	1	Si-N Si-O-Si	89α:11β		1940 °C, 2 h, 2.2 MPa N_2	64β^1:36α^1 Melilite	97.59	0.16	
A1	Water	7	1	Si-N Si-O-Si	89α:11β		1940 °C, 2 h, 2.2 MPa N_2	75β^1:25α^1 Melilite	99.70	1.32	–
B2	Water	4	3	Si-N Si-O-Si	100β	Si	1940 °C, 2 h, 2.2 MPa N_2	78β^1:22α^1 Melilite	99.99	3.66	14.34
B1	Isopropanol	9	4	Si-N Si-O-Si	100β	Si	1940 °C, 2 h, 2.2 MPa N_2	73β^1:27α^1 Melilite	99.90	2.57	17.00
B0.5	Water	21	8	Si-N Si-O-Si OH	100β	Si, SiO_2	1940 °C, 2 h, 2.2 MPa N_2	100β^1 Amorphous	99.46	7.28	18.40
B0.5	Water	21	8	Si-N Si-O-Si OH	100β	Si, SiO_2	1850 °C, 1 h, 2.2 MPa N_2	100β^1 Amorphous	98.90	3.70	–

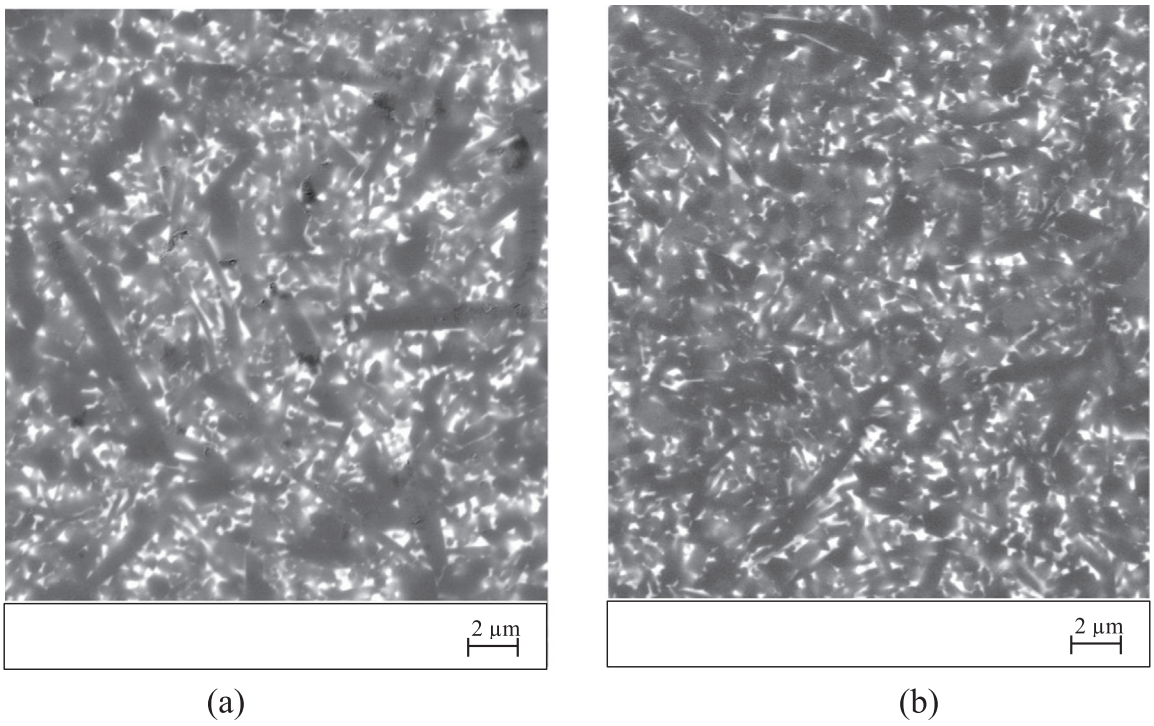

Fig. 7. SEM-BSE images of (a) R and (b) A1 powders containing compositions sintered at 1940 °C, for 2 h.

with a high aspect ratio of 10 were grown from the supersaturated liquid phase. Besides, since the solubility of the R powder was greater with respect to the A1 powder containing composition, the quantity of the high temperature liquid phase formed was larger. In the A1 composition the evolution of needle like 5–7 μm long, 0.8–1 μm wide β-SiAlON grains with the aspect ratio larger than 7 was observed.

The microstructural development of the compositions prepared by the β-Si_3N_4 powders of various initial mean particle sizes (B2, B1, B0.5) was given in Fig. 8. The coarser powder (B2) yielded SiAlON grains with diameters 1–5 μm and aspect ratios in the range 2–3 as shown in Fig. 8a. When the β-Si_3N_4 powder with the mean particle size of 1 μm was used, the diameter of the SiAlON grains was approximately 1 μm and the aspect ratio increased to the range 2.5–4.5 as shown in Fig. 8b. The B0.5 powder which had the finest mean particle size yielded 2 μm diameter and 7–8 aspect ratio β^1-SiAlON grains in a nano sized matrix (Fig. 8c).

It was clear that the microstructural evolution of the SiAlON ceramics produced from the β-Si_3N_4 powders depended on the particle size of the initial β-Si_3N_4 powder. The microstructures evolved from the coarser β-Si_3N_4 powders (B2 and B1) were coarser, but the fine β-Si_3N_4 powder (B0.5) yielded a bimodal microstructure. In the literature similar results were obtained with the sintering of powders at 1850 °C, for 5 h, under 0.1 MPa N_2 gas atmosphere. While the coarser initial powder of 0.66 μm mean particle yielded a microstructural evolution

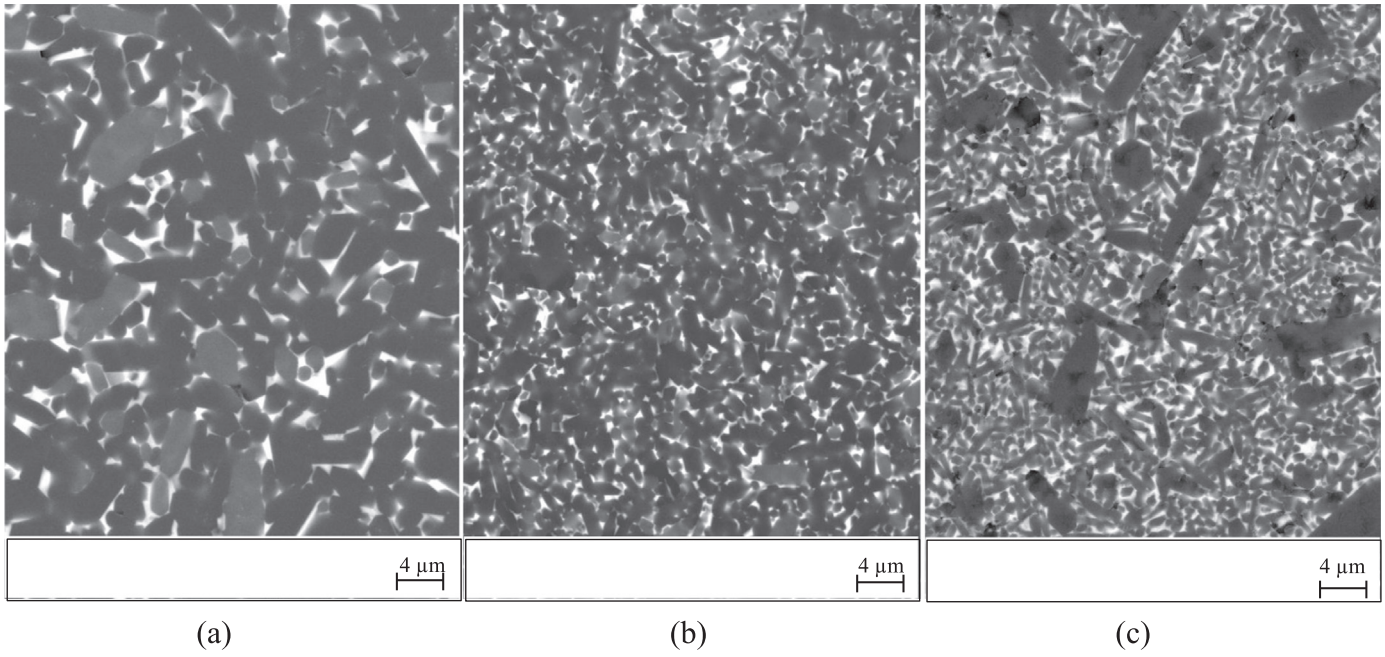

Fig. 8. SEM-BSE images of (a) B2, (b) B1, (c) B0.5 powders containing compositions sintered at 1940 °C for 2 h.

with equiaxed grains, the finer powders of mean particle sizes of 0.44 μm and 0.26 μm yielded needle like grain growth in a fine matrix. The grain growth rate increased with the decreasing initial particle size, consistent with the present work [18,44].

The SiAlON grains developed from the β-Si_3N_4 powder by the β-Si_3N_4 grain dissolution in the liquid phase and precipitation to the thermodynamically stable phase. The seeding could have been by the homogeneous seeding from the liquid or by the heterogeneous seeding on the β-Si_3N_4 crystals [19]. The development of a coarser microstructure from a coarser β-Si_3N_4 powder and a finer microstructure from a finer β-Si_3N_4 powder provided evidence that the heterogeneously dispersed, undissolved β-Si_3N_4 crystals provided the seeding. This was attributed to the fast rate of β-Si_3N_4→α^1-SiAlON transformation and fast rate of dissolution of the initial crystals in the liquid phase with the finer (1 μm) initial β-Si_3N_4 powder. However, when coarser particle size β-Si_3N_4 powder was used the transformation and the seeding frequency were slower causing equiaxed grain growth. As a result, since the coarse β-Si_3N_4 powders (B2 ve B1) were rather stable, the grains were not completely dissolved during sintering, and the final grain size was proportional with the initial particle size. The critical particle diameter of the β-Si_3N_4 powder for the formation of needle like SiAlON grains was determined to be less than 0.5 μm.

The microstructures obtained by the sintering of the R and the B0.5 compositions at 1850 °C for 1 h are given in Fig. 9a,b. Both compositions yielded nano sized grain growth. However, since the B0.5 powder included a little amount of large particles, in the final sintered microstructure the development of high diameter (~2 μm) and low aspect ratio (~2) β^1-SiAlON grains was observed as seen in Fig. 9a. The β^1-SiAlON grains of the matrix were needle like with diameter of ~0.2 μm, length of 1.4 μm and aspect ratio of ~7. The microstructure obtained by the sintering of the R powder contained grains with diameter of 3 μm and aspect ratio of 11 dispersed among nano sized α^1-SiAlON particles. While in the sintered B0.5 powder containing composition, the amorphous grain boundary phase was dispersed homogeneously, the R composition yielded crystalline grain boundary phase that was lumped at positions dispersed heterogeneously because of the fusing of the melilite transition phase at the sintering temperature. Also due to the insufficient liquid phase formation during sintering pores existed in the microstructure. This result showed that in the production of a dense material, not only the particle size and polymorphic type of the initial Si_3N_4 powder were effective, but the liquid phase composition during the maximum sintering temperature proved effective, as well. In the Sm rich compositions the densification was adversely affected, since the formation of the melilite phase crystallization was extensive.

When the R and the B0.5 compositions were sintered at 1940 °C needle like, high aspect ratio grain growth was obtained as shown in Fig. 7a and Fig. 8c. When the same compositions were sintered at a lower temperature of 1850 °C grain growth did not occur and the evolved microstructure was fine (Fig. 9a, b). This provided evidence that the grain growth was induced not only by the initial powder particle size, but by the sintering temperature as well.

4. Conclusions

In this study, the correlation of the surface characteristics of the Si_3N_4 powder and the sintering behavior, and the phase assemblages was determined. The prominent points are as follows. As revealed by FTIR analysis milling of β-Si_3N_4 powder in water for 21 h led to the formation of OH groups on Si_3N_4 powder surfaces. For the B0.5 powder shift of Si-N band ranges from 835 to 814 cm^{-1} to 925 cm^{-1} took place after 21 h milling in water, which was related to the SiO_2 formation on Si_3N_4 powder surfaces. The formation of SiO_2 on the β-Si_3N_4 particles resulted in denser sintered products. The milling of the α-Si_3N_4 powder in isopropanol for 9 h had no effect on the surface groups.

The initial particle size had crucial importance on the microstructural evolution. The coarser Si_3N_4 powders resulted in coarser α^1:β^1-SiAlON microstructure. Independent of the polymorphic type of the Si_3N_4 powder (α or β), finer microstructure development was obtained when the starting powder had finer particle size, and vice versa coarser microstructure development was obtained when the starting powder was coarser. Since the β-Si_3N_4 powder was stable even at high temperatures α→β-Si_3N_4 transformation did not take place, and hence the bimodal microstructural development was controllable with the initial particle size. In the case that the particle size was up to 0.5 μm,

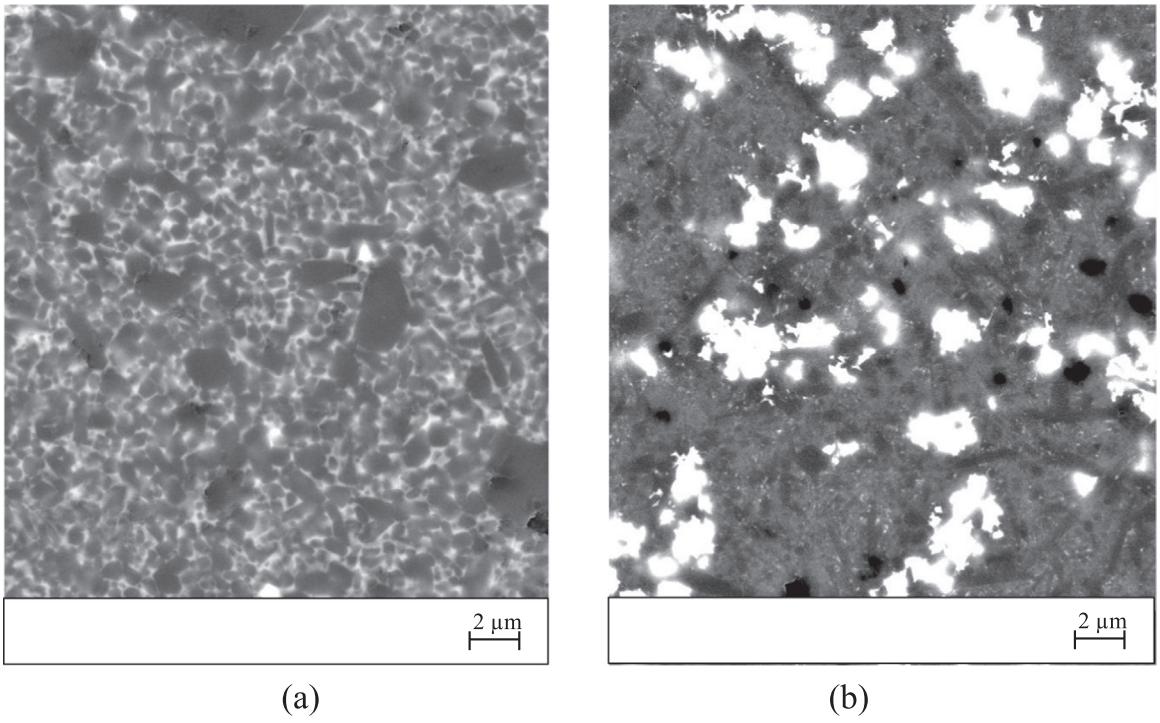

Fig. 9. SEM-BSE images of (a) B0.5 and (b) R powders containing compositions sintered at 1850/ °C for 1 h.

the particles were formed with the dissolution-precipitation process, and bimodal microstructural development took place with the homogeneous seeding from the liquid phase. Otherwise the coarser particles were rather stable rendering the grain growth to occur from the existing crystals which had formed by heterogeneous seeding, and yielding coarser microstructural development depending on the particle size of the initial powder. In obtaining the designed α^1:β^1-SiAlON phase ratios, the milling conditions of the powder proved prominent. Excess milling period and speed resulted in the oxidation of the Si_3N_4 powders, and the composition shifted into the β^1-SiAlON region, increasing the grain boundary phase quantity.

References

[1] C.B. Carter, M.G. Norton, Ceramic Materials Science and Engineering, Springer-Verlag, New York, 2013.
[2] D.V. Richerson, Modern Ceramic Engineering: Properties, Processing, and Use in Design, third ed, CRC Press, Taylor and Francis Group, 2005.
[3] J.F. Collins, R.W. Gerby, New refractory uses for silicon nitride reported, J. Met. 7 (1955) 612–615.
[4] G.R. Terwilliger, Properties of sintered Si_3N_4, J. Am. Ceram. Soc. 57 (1974) 48–49.
[5] T. Ekström, M. Nygren, SiAlON ceramics, J. Am. Ceram. Soc. 75 (1992) 259–276.
[6] K.H. Jack, W.J. Wilson, Ceramics based on the Si-Al-O-N and related systems, Nat. (Phys. Sci.) 238 (80) (1972) 28–29.
[7] S. Boskovic, K.G. Nickel, G. deWith, R.A. Terpstra, R. Metselaar (Eds.), Preparation and Properties of α:β SiAlON Composites, Euro Ceramics Volume I, Elsevier Applied Science, London, 1989, p. 441.
[8] F. Riley, Silicon nitride and related materials, J. Am. Ceram. Soc. 83 (2000) 245–265.
[9] N. Calis Acikbas, S. Tegmen, S. Ozcan, G. Acikbas, Thermal shock behaviour of α:β-SiAlON-TiN composites, Ceram. Int. 40 (2014) 3611–3618.
[10] S.R. Kushan, I. Uzun, B. Dogan, H. Mandal, Experimental and finite element study of the thermal conductivity of α-SiAlON ceramics, J. Am. Ceram. Soc. 90 (12) (2007) 3902–3907.
[11] B. Basu, J. Vleugels, M. Kalin, O. Van Der Biest, Friction and wear behaviour of SiAlON ceramics under fretting contacts, Mater. Eng. A 359 (2003) 228–236.
[12] R. Kumar, N. Calis Acikbas, F. Kara, H. Mandal, B. Basu, Microstructure-mechanical properties-wear resistance relationship of SiAlON ceramics, Metall. Mater. Trans. A (2009) 2319–2332.
[13] H. Mandal, N. Calis Acikbas, Processing, characterization and mechanical properties of SiAlONs produced from low cost β-Si3N4 powder, KONA Powder Part. J. 30 (2013) 22–30.
[14] N. Calis Acikbas, R. Kumar, F. Kara, H. Mandal, B. Basu, Influence of β-Si3N4 particle size and heat treatment on microstructural evolution α:β-SiAlON ceramics, J. Eur. Ceram. Soc. (2011) 629–635.
[15] N. Calis Acikbas, F. Kara, H. Mandal, Development of α-β SiAlON ceramics from different $Si3N_4$ starting Powders, Key Eng. Mater. (2009) 107–108.
[16] M. Mitomo, H. Hirotsuru, H. Suematsu, T. Nishimura, Fine-grained silicon nitride ceramics prepared from □-powder, J. Am. Ceram. Soc. 78 (1995) 211–214.
[17] S.K. Lee, K.S. Lee, B.R. Lawn, D.K. Kim, Effect of starting powder on damage resistance of silicon nitrides, J. Am. Ceram. Soc. 81 (1998) 2061–2070.
[18] C.J. Lee, J.I. Chae, D.J. Kim, Effect of □-Si3N4 starting powder size on elongated grain growth in □-Si3N4 ceramics, J. Eur. Ceram. Soc. 20 (2000) 2667–2671.
[19] T. Ekström, N. Ingelström, R. Brage, M. Hatcher, T. Johansson, α-β-SiAlON ceramics made from different silicon nitride powders, J. Am. Ceram. Soc. 71 (1988) 1164–1170.
[20] Y.W. Li, P.L. Wang, W.W. Chen, Y.B. Cheng, D.S. Yan, Phase formation and microstructural evolution of Ca α-SiAlON using different Si3N4 starting powders, J. Eur. Ceram. Soc. 20 (2000) 1803–1808.
[21] J.Q. Dai, Y. Huang, J.T. Ma, Surface characteristics and aqueous dispersibility of commercial silicon nitride powders: effects of acid leaching, surface hydrolysis and thermal oxidation, Ceram. Int. 34 (2008) 1835–1842.
[22] Y. Huang, J. Dai, Z. Xie, T. Ma, J. Yang, J. Ma, Effects of liquid medium and ball milling on the surface group and aqueous dispersibility of Si3N4 powder, J. Eur. Ceram. Soc. 23 (2003) 985–990.
[23] O. Tapaszto, C. Balazsi, The efeect of milling time on the sintering kinetics of Si3N4 based nanocomposites, Ceram. Int. 36 (2010) 2247–2251.
[24] N. Calis Acikbas, O. Demir, The effect of cation type, intergranular phase amount and cation mole ratios on z value and intergranular phase crystallisation of SiAlON ceramics, Ceram. Int. 39 (2013) 3249–3259.
[25] N. Calis Acikbas, H. Yurdakul, H. Mandal, F. Kara, S. Turan, A. Kara, B. Bitterlich, Effect of sintering conditions and heat treatment on the properties, microstructure and machining performance of α:β-SiAlON ceramics, J. Eur. Ceram. Soc. (2012) 1321–1327.
[26] N. Calis Acikbas, A. Kara, S. Turan, F. Kara, H. Mandal, B. Bitterlich, Influence of type of cations on intergranular phase crystallisation of SiAlON ceramics, Mater. Sci. Forum (2007) 119–122.
[27] N. Calis Acikbas, H. Mandal, The fluorine effect on the grain-growth of α^1:β^1-sialon ceramics, Anadolu Univ. J. Sci. Technol. A – Appl. Sci. Eng. 17 (5) (2016) 895–904.
[28] K. Liddell, X-ray Analysis of Nitrogen Ceramic Phases (MSc thesis), University of Newcastle upon Tyne, UK, 1979.
[29] T.K. Trout, J.M. Bellama, F.E. Brinckman, R.A. Faltynek, Fourier transform infrared analysis of ceramic powders: quantitative determination of alpha, beta, and amorphous phases of silicon nitride, J. Mater. Res. 4 (2) (1989) 399–403.
[30] J.C. Bressiani, V. Izhevskyi, A.H.A. Bressiani, Development of the microstructure silicon nitride based ceramics, Mater. Res. 2 (1999) 165–172.
[31] E.L. Boris, V. Zhmud, L. Bergstrom, Dissolution and deagglomeration of silicon nitride in aqueous medium, J. Am. Ceram. Soc. 83 (2000) 2394–2400.
[32] S.-H. Rhee, J.-D. Lee, D.Y. Kim, Effect of α-Si3N4 initial particle size on the microstructural evolution and phase transformation during sintering of Si3N4 ceramics, J. Eur. Ceram. Soc. 20 (2000) 1787–1794.
[33] C. He, Y.S. Wang, J.S. Wallance, S.M. Hsu, Effect of microstructure on the wear transition of zirconia-toughened alumina, Wear 162–164 (1993) 314–321.
[34] O.O. Ajayi, K.C. Ludema, Surface damage of structural ceramics: implications for wear modelling, Wear 124 (1988) 237–257.
[35] K.H. Zum Gahr, W. Bundschuh, B. Zimmerlin, Effect of grain size on friction and sliding wear of oxide ceramics, Wear 162–164 (1993) 269–279.
[36] A.K. Mukhopadhyay, Y.-W. Mai, Grain size effect on abrasive wear mechanisms in alumina ceramics, Wear 162–164 (1993) 258–268.
[37] M.R. Miranda-Martinez, W. Davidge, F.L. Riley, Grain size effects on the wet erosive wear of high purity polycrystalline alumina, Wear 172 (1994) 41–48.
[38] R.W. Davidge, F.L. Riley, Grain size dependence of the wear of alumina, Wear 186–187 (1995) 45–49.
[39] J. Sedlacek, D. Galusek, P. Svancarek, R. Riedel, A. Atkinson, X. Wang, Abrasive wear of Al2O3-SiC and Al2O3-(SiC)-C composites with micrometer and submicrometer sized alumina matrix grains, J. Eur. Ceram. Soc. 28 (2008) 2983–2993.
[40] R.S. Roy, D. Basu, A. Chanda, M.K. Mitra, Distinct wear characteristics of submicrometer grained alumina in air and distilled water: a brief analysis on experimental observation, J. Am. Ceram. Soc. 90 (2007) 2987–2991.
[41] C.P. Dogan, J.A. Hawk, Role of composition and microstructure in the abrasive wear of high alumina ceramics, Wear 225–229 (1999) 1050–1058.
[42] C.P. Dogan, J.A. Hawk, Microstructure and abrasive wear in silicon nitride ceramics, Wear 250 (2001) 256–263.
[43] M. Herrmann, I. Schulz, C. Schubert, W. Hermel, D.I. Zalite, G. Ziegler, Ultrafine Si3N4 materials with low coefficients of friction and wear rates, Ceram. Forum Int. 75 (1998) 38–45.
[44] A. Rosenflanz, α-SiAlON: Phase Stability, Phase Transformations and Microstructural Evolutions (Ph.D. Thesis), Michigan University, Michigan, USA, 1997, pp. 178–179.